RSC Advances

PAPER

View Article Online
View Journal | View Issue

Cite this: *RSC Adv.*, 2020, **10**, 43109

Facile construction of a flexible and wearable electrode based on the hierarchical structure of RGO-coated cotton fabric with amorphous Co–Ni–B alloy

Wei Wang, *[a] Jishu Zhang,[a] Tao Li[a] and Shuo Wang*[bc]

Received 13th August 2020
Accepted 12th November 2020

DOI: 10.1039/d0ra06988d

rsc.li/rsc-advances

As an emerging energy storage material, amorphous Co–Ni–B alloy was firstly introduced to construct the flexible supercapacitor electrode. To ensure the high electrochemical property, amorphous Co–Ni–B alloy and RGO sheets were combined to form the three-dimensional hierarchical structure on the surface of the cotton fabric, which was beneficial to enhance the electrochemical property. Notably, the preparation conditions of this amorphous Co–Ni–B/RGO/fabric electrode were facile and mild with room temperature and atmospheric pressure, thus avoiding serious damage to the textile fabric because of high temperature and harsh chemical reactions of most preparation methods. This flexible electrode exhibited an optimum specific capacitance of 313.9 F g^{-1} at 5 mV s^{-1} and good cycling stability with specific capacitance retention of 85.0% after 3000 cycles. Such special architecture bestowed this electrode with nice electrochemical property, in addition to great promising application in the supercapacitor field.

Introduction

Substantial efforts have been made in the research of flexible supercapacitors to meet the rapid development of wearable electronic devices because flexible supercapacitors exhibit outstanding mechanical flexibility, long lifespan, and high power capability.[1–4] The electrochemical property of the supercapacitor is mainly determined by the performance of the corresponding electrode material. Although a considerable mass of electric double-layer and pseudo-capacitive materials were developed for textile electrodes, the preparation methods for most of the flexible electrodes are complicated, time-consuming, and harsh,[5–10] requiring high temperature, long time, or hazardous solvent. Therefore, it is vital to explore the novel electrode materials with high performance, in addition to the facile, mild, and cost-effective preparation method.

Very recently, amorphous transition metal borides (TMBs) have emerged as more attractive pseudocapacitive materials due to their excellent electrochemical activity, special crystal feature, as well as good thermal stability. The metastable crystal structure, inherent defects, and sufficient ion diffusion channels resulted from the disordered long-range atomic arrangement, which endows amorphous TMBs with the improved electrochemical property. Therefore, the application of TMBs has been expanded to the energy harnessing field from luminescence, thermoelectric, and magnetic field.[11–13] For example, the specific capacitance of amorphous Ni–Co–B was measured to be 2226.96 F g^{-1} with a current density of 1 A g^{-1}.[12] Amorphous Co–Fe–B showed a good specific capacitance of 981 F g^{-1} at the current density of 1 A g^{-1}.[13] Both of these flexible electrodes exhibited splendid electrochemical characteristics. Moreover, the preparation routes of these TMBs are simple, mild, and cost-effective, only requiring 10 min for the chemical reaction at room temperature and normal pressure. With these excellent properties, TMBs will be one of the most promising electrode materials, and hence an in-depth study is important. However, only a few reports have focused on the research of the electrochemical performance of TMBs. Accordingly, the binder-free composite electrodes fabricated with TMBs for flexible supercapacitors have rarely been reported.

Cotton fabrics possess intrinsic flexibility, porous structure, lightweight, low-cost, biocompatibility, and comfortable sensation; thus, they have been regarded as an ideal platform for a future flexible electrode.[14–18] However, the electrodes prepared just with TMBs and cotton fabric possessed low electrochemical conductivity, poor cycling stability, and low power density due to the insulating property of the cotton fabric and required to integrate extra conductive materials.[19,20] In this regard, carbon materials like carbon nanotube and graphene are often introduced as conductive and double-layer materials to improve electrochemical

[a]*College of Textile & Garment Engineering, Changshu Institute of Technology, Suzhou, 215500, China. E-mail: wangweiwei8660@126.com*

[b]*College of Textiles and Garments, Hebei University of Science and Technology, Shijiazhuang, 050018, China. E-mail: fzwangshuo@hebust.edu.cn*

[c]*Hebei Technology Innovation Center of Textile and Garment, Shijiazhuang, 050018, China*

features.[21] As one of the typical TMBs, amorphous Co–Ni–B has demonstrated its tempting pseudocapacitive storage properties.[11] With these favorable features, amorphous Co–Ni–B was coupled with carbon materials to construct a hierarchical structure to impart cotton fabric the nice electrochemical property. Herein, the cotton fabric with a hierarchical 3D porous structure was primarily used as a structural backbone. In detail, the dipping-drying method and chemical reduction method were adopted to prepare this Co–Ni–B/RGO/fabric composite electrode. Based on the aforementioned analysis, these preparation conditions were mild and easy to control with room temperature, normal pressure, and short reaction time, and were suitable for mass production. Moreover, these conditions effectively avoid the damages to the cotton fabric comparable to the high temperature and harsh chemical reactions of most preparation methods.

Experimental

Materials

Cobalt nitrate hexahydrate ($Co(NO_3)_2 \cdot 6H_2O$), nickel nitrate hexahydrate ($Ni(NO_3)_2 \cdot 6H_2O$), sodium borohydride ($NaBH_4$), sodium hydroxide (NaOH), and sodium sulfate (Na_2SO_4) were purchased from Sinopharm Chemical Reagent Co., Ltd and used without any further purification. Graphene oxide (GO) was purchased from Beijing Boyu Co., Ltd. Woven cotton fabric was purchased from Shaoxing Aobang Textile Company.

Fabrication of RGO/cotton fabric electrode

RGO/cotton fabric electrode was produced with the dip-drying method according to the previous report.[22] GO powder (0.1 g) was added into 50 mL of double-distilled water and stirred for 30 min. Then, the suspension was sonicated for 30 min to ensure the complete dispersion of GO. Moreover, the cotton fabric was treated with 1 mol L^{-1} of NaOH aqueous solution at 100 °C for 1 h to remove impurities and grease. Afterward, the clean cotton fabric was placed into the aforementioned GO dispersion for 30 min at room temperature and dried at 60 °C for 2 h. To increase the payload of GO, this process was repeated ten times. After that, GO/cotton fabric was immersed into 0.6 mol L^{-1} of $NaBH_4$ for 6 h to reduce GO to RGO.

Fabrication of amorphous Co–Ni–B/RGO/cotton fabric electrode

Co–Ni–B/RGO/cotton fabric electrode was prepared based on Meng's report.[11] In detail, $Co(NO_3)_2 \cdot 6H_2O$ powders and $Ni(NO_3)_2 \cdot 6H_2O$ powders were firstly mixed under vigorous stirring in 100 mL deionized water to obtain uniform dispersion (solution A). Another 25 mmol of $NaBH_4$ and 5 mmol of NaOH were mixed into 50 mL deionized water for 10 min (solution B). After that, RGO/cotton fabric with a size of 1 × 2 cm^2 was dipped into solution A for 30 min. Solution B was then added into solution A drop by drop. The mixed solution was then stirred for another 10 min. Afterward, the treated cotton fabric was taken out and carefully washed with doubly distilled water and ethanol. Finally, Co–Ni–B/RGO/cotton fabric electrode was obtained after being dried at 60 °C for 12 h. The molar ratio of $Co(NO_3)_2 \cdot 6H_2O$ to $Ni(NO_3)_2 \cdot 6H_2O$ was adjusted from 1 : 2 to 1 : 1 to 2 : 1, which was denoted as Co1–Ni2–B/RGO/cotton fabric, Co1–Ni1–B/RGO/cotton fabric, and Co2–Ni1–B/RGO/cotton fabric, respectively.

General characterization

The surface morphology of this electrode was examined with a scanning electron microscope (SEM, SU8010, Hitachi) and a transmission electron microscope (TEM, JEM-2100). The elemental distribution was observed using elemental mapping and energy dispersive spectrometer (SEM-EDS). The selected area electron diffraction (SAED) patterns from HR-TEM measurement and X-ray diffractometer (XRD) were employed to confirm the crystalline structure of Co–Ni–B alloy. X-ray photoelectron spectrometer (XPS, Thermo Scientific Escalab, USA) was used to analyze the element compositions and chemical bonding states of these electrodes. Electrochemical properties of these electrodes were analyzed by cyclic voltammogram (CV) curve, galvanostatic charge/discharge curve (GCD), and electrochemical impedance spectra (EIS) with three-electrode configuration system (CHI660E Instruments, Chenhua Instruments Corporation, Shanghai). Specifically, the resultant fiber electrode with a size of 1 cm × 1 cm, Ag/AgCl electrode, and Pt foil was used as a working electrode, reference electrode, and counter electrode, respectively. Na_2SO_4, with a concentration of 1 mol L^{-1}, was used as an electrolyte. The specific capacitance of these electrodes was obtained according to the following equation:

$$C = \frac{1}{sm\Delta V}\int_{v_0}^{v_0+\Delta V} i\,dV \quad (1)$$

where C is the specific capacitance, s is the scan rate, m is the active material mass, and ΔV is the voltage window.

$$C = (I \times \Delta t)/(\Delta V \times m) \quad (2)$$

where C is the specific capacitance, I is the discharge current (A), Δt is discharge time (s), ΔV is voltage window, and m is the mass (g) of the active electrode materials.

Results and discussion

The preparation process diagram of Co–Ni–B/RGO/cotton fabric composite electrode is presented in Fig. 1. The RGO/cotton

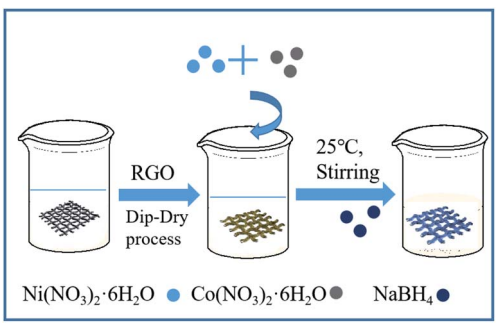

Fig. 1 The schematic diagram of the preparation process of Co–Ni–B/RGO/cotton fabric composite electrode.

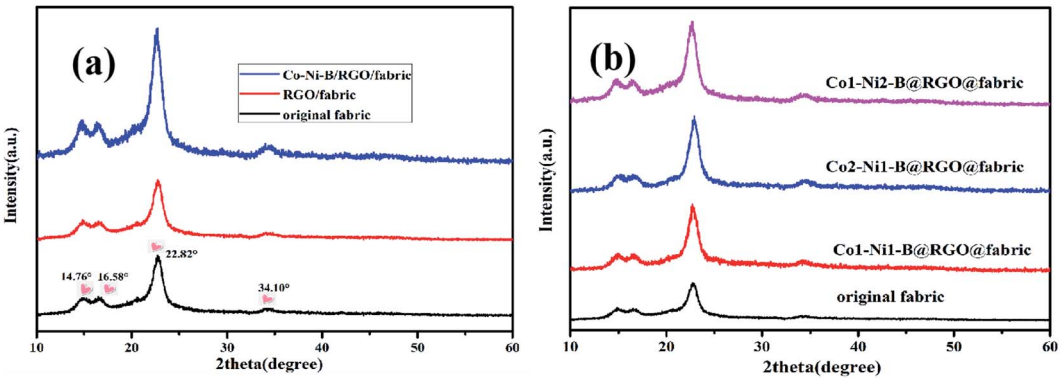

Fig. 2 XRD patterns: (a) original fabric, RGO/fabric, and Co–Ni–B/RGO/fabric; (b) original fabric and Co-Ni-B/RGO/fabric with different molar ratio of Co^{2+}/Ni^{2+}.

fabric composite with a size of 1 × 2 cm^2 was firstly prepared through the dip-drying method. In detail, the cotton fabric was impregnated in 2 g L^{-1} of GO solution for 10 cycles, and each dipping time was 30 min. Then, GO was reduced to RGO with a $NaBH_4$ solution of 0.6 mol L^{-1}. After that, RGO/fabric was immersed in the mixture solution containing $Co(NO_3)_2 \cdot 6H_2O$ and $Ni(NO_3)_2 \cdot 6H_2O$ in different molar ratios for 10 min. Subsequently, the aqueous solution containing NaOH and $NaBH_4$ was cautiously added drop by drop. After reacting for 10 min, the Co–Ni–B/RGO/fabric electrode was taken out and washed several times with doubly distilled water and ethanol. Finally, the as-made sample was dried at 60 °C for 12 h.

Fig. 2a shows the crystal structure of the original fabric, RGO/cotton fabric, and Co–Ni–B/RGO/cotton fabric composite

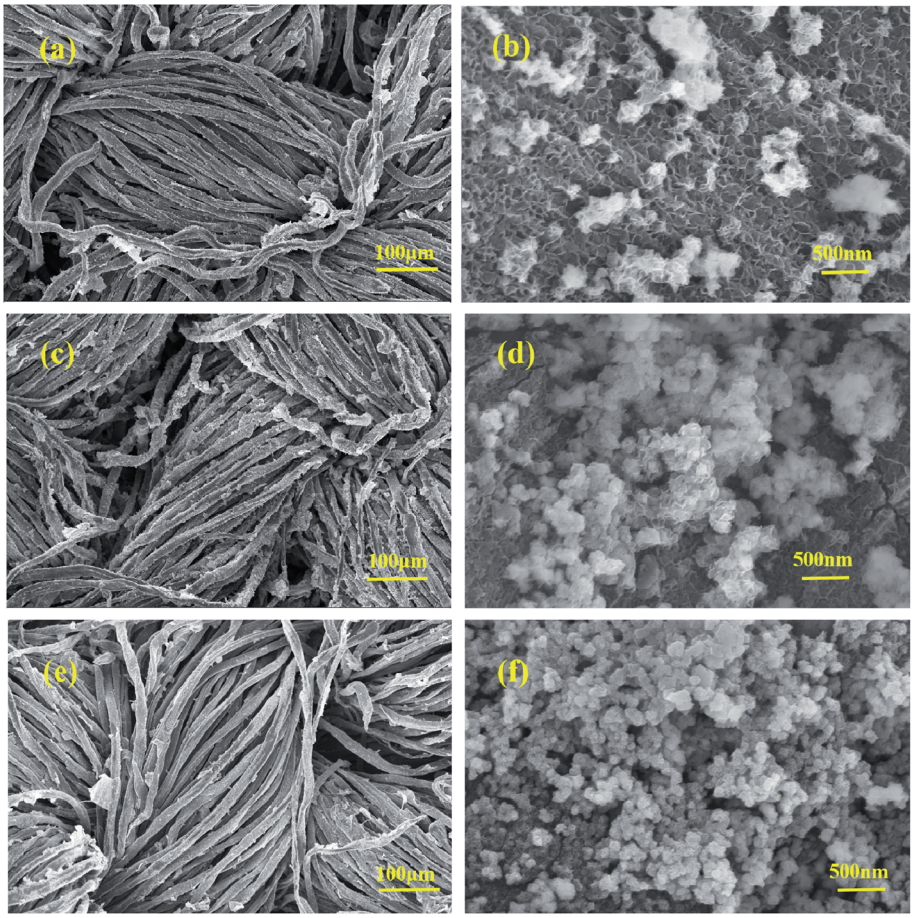

Fig. 3 SEM images with different magnifications: Co2–Ni1–B/RGO/cotton fabric (a and b); Co1–Ni1–B/RGO/cotton fabric (c and d); Co1–Ni2–B/RGO/cotton fabric (e and f).

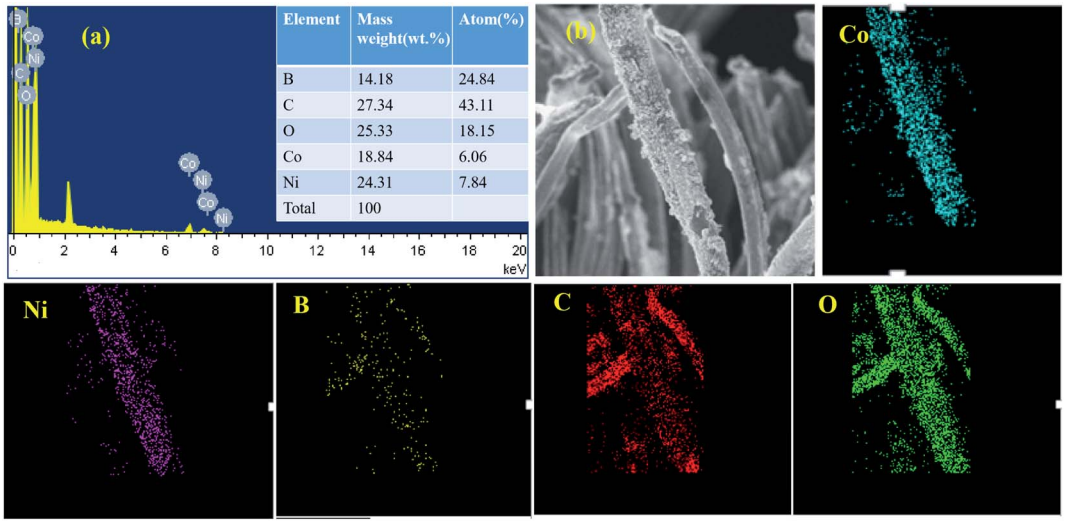

Fig. 4 (a) EDS images with molar ratio of Co1–Ni1–B/RGO/cotton fabric and its corresponding mapping test (b).

electrode. The XRD patterns of diffraction peaks at $2\theta = 14.76°$, 16.58°, 22.82°, and 34.10° exhibited typical cellulose I characteristics of the cotton fabric.[23] After being coated with RGO and Co–Ni–B alloy, no new diffraction peaks were observed due to their low amount compared with that of the cotton fabric substrate. Even after changing the molar ratio of Co^{2+}/Ni^{2+}, no new peaks can be seen in Fig. 2b. The forming mechanism of Co–Ni–B was explained by the following reactions.[24,25]

$$BH_4^- + 3Co^{2+} + 3H_2O \leftrightarrow BO_2^- + 3Co + 2H_2 + 6H^+ \quad (3)$$

$$BH_4^- + 3Ni^{2+} + 3H_2O \leftrightarrow BO_2^- + 3Ni + 2H_2\ 6H^+ \quad (4)$$

$$BH_4^- + 3H_2O \leftrightarrow B + 2.5H_2 + OH^- \quad (5)$$

The morphologies of Co–Ni–B/RGO/fabric composite electrodes with different Co/Ni molar ratios, examined with SEM, are shown in Fig. 3. In our previous report, the surface of RGO/cotton fabric was covered by a wrinkled RGO sheet of several micrometers.[20] The SEM images with low-magnification (Fig. 3a, c, and e) confirmed that Co–Ni–B nanograins were uniformly grown on the surface of the RGO/fabric composite. However, the SEM images of high magnification revealed that

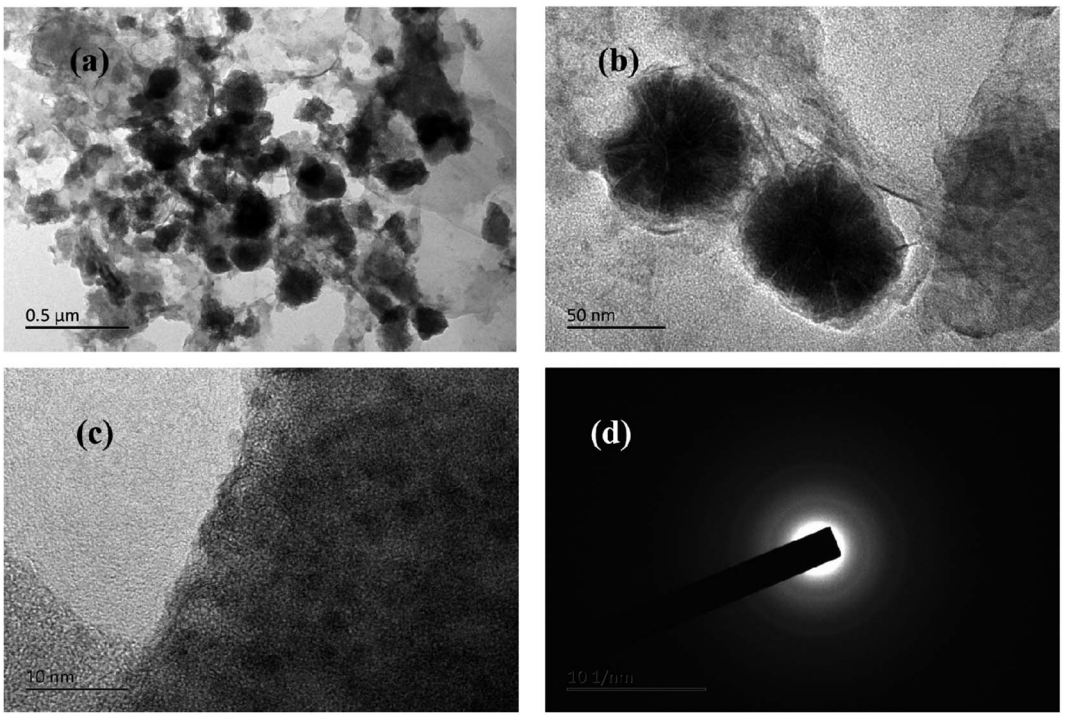

Fig. 5 TEM images of Co1–Ni1–B/RGO/fabric (a and b) TEM images, (c) HRTEM Image, and (d) SAED pattern.

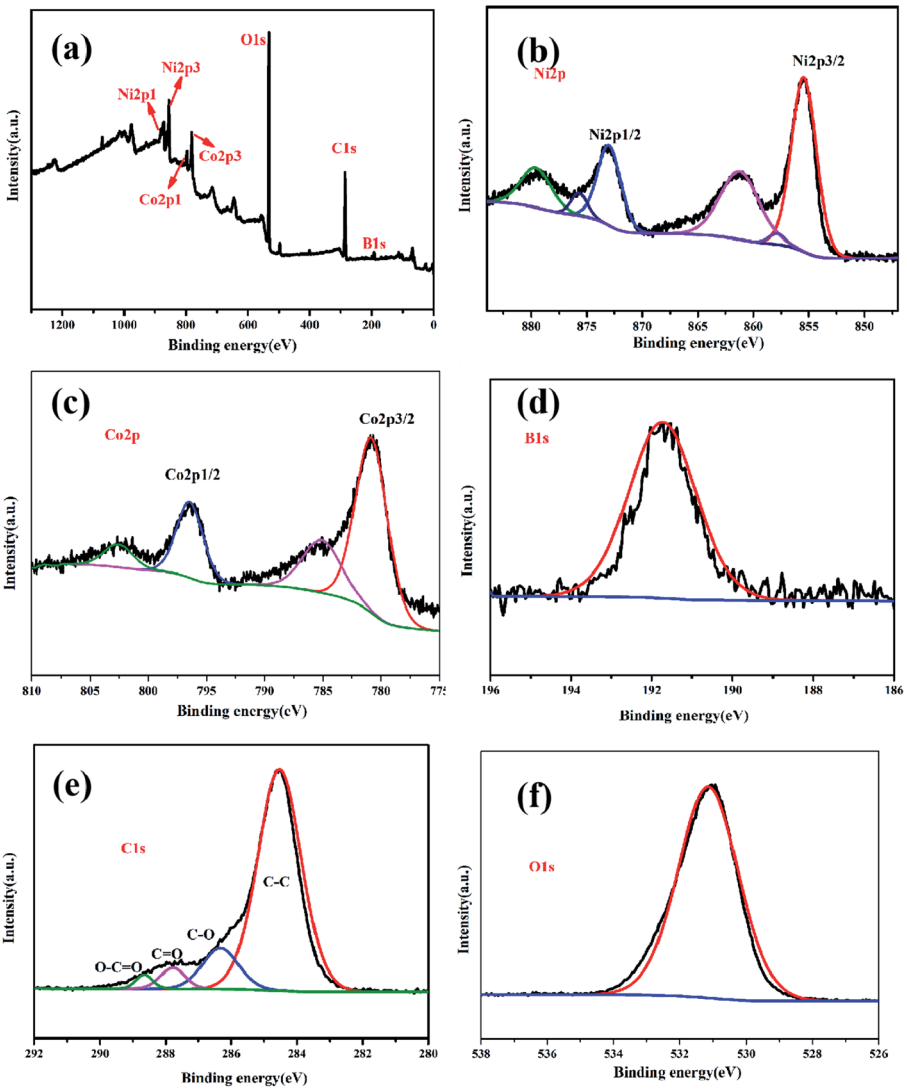

Fig. 6 The full scan XPS spectra of Co1–Ni1–B/RGO/fabric electrode (a); high-resolution XPS spectra of Ni 2p (b), Co 2p (c), B 1s (d) C 1s (e), and O 1s (f).

these nanograins were composed of numerous particles, as shown in Fig. 3b, d, and f. With the ratio of Co^{2+}/Ni^{2+} as 2 : 1, this electrode exhibited the sheet structure, along with a partial nanoparticle agglomeration (Fig. 3b). Upon changing the Co^{2+}/Ni^{2+} to 1 : 1, this electrode showed many nanoparticles with intertwined nanoflakes, as displayed in Fig. 3d. The disordered arrangement of nanoflakes brought about plenty of void spaces, similar to a network. The three-dimensional hierarchical structure on the surface of the cotton fabric was beneficial for improving the kinetics.[13,26] When Co^{2+}/Ni^{2+} ratio was 1 : 2, the sizes of these nanoparticles with intertwined nanoflakes decreased compared with those of the composite electrode prepared with Co^{2+}/Ni^{2+} of 1 : 1. Obviously, the microstructure of this electrode depends on the molar ratio of Co^{2+}/Ni^{2+}, thus affecting its electrochemical performance.

The mapping test clarified that B, Ni, Co, C, and O elements all existed in this composite. The Co/Ni molar ratio was measured nearly 1 : 1.29, which corresponded to Co1–Ni1–B/RGO/fabric electrode from the EDS test (Fig. 4a). Moreover, the elemental mapping method was adopted to analyze the elemental distribution on the surface of this fabric electrode. From Fig. 4b, it was observed that five elements, Co, Ni, B, C, and O, were uniformly distributed, suggesting that Co–Ni–B alloy was successfully attached on the surface of the RGO/fabric composite electrode.

The typical TEM images of Co1–Ni1–B/RGO composite were captured to examine the structural units on the surface of Co1–Ni1–B/RGO/cotton fabric. Fig. 5a and b shows that flower-shaped nanoparticles of 50–60 nm, which scraped off from the cotton fabric composed of numerous Co–Ni–B nanosheets, were tightly anchored on the graphene sheets, with the result being consistent with those of SEM images. The HR-TEM image of Fig. 5c displayed that no obvious crystal lattice was detected, thereby demonstrating that Co1–Ni1–B alloy had an amorphous structure. In addition, the selected area electron diffraction pattern in Fig. 5d demonstrated the amorphous structure of Co–Ni–B with diffused and broad rings. This result was consistent with the

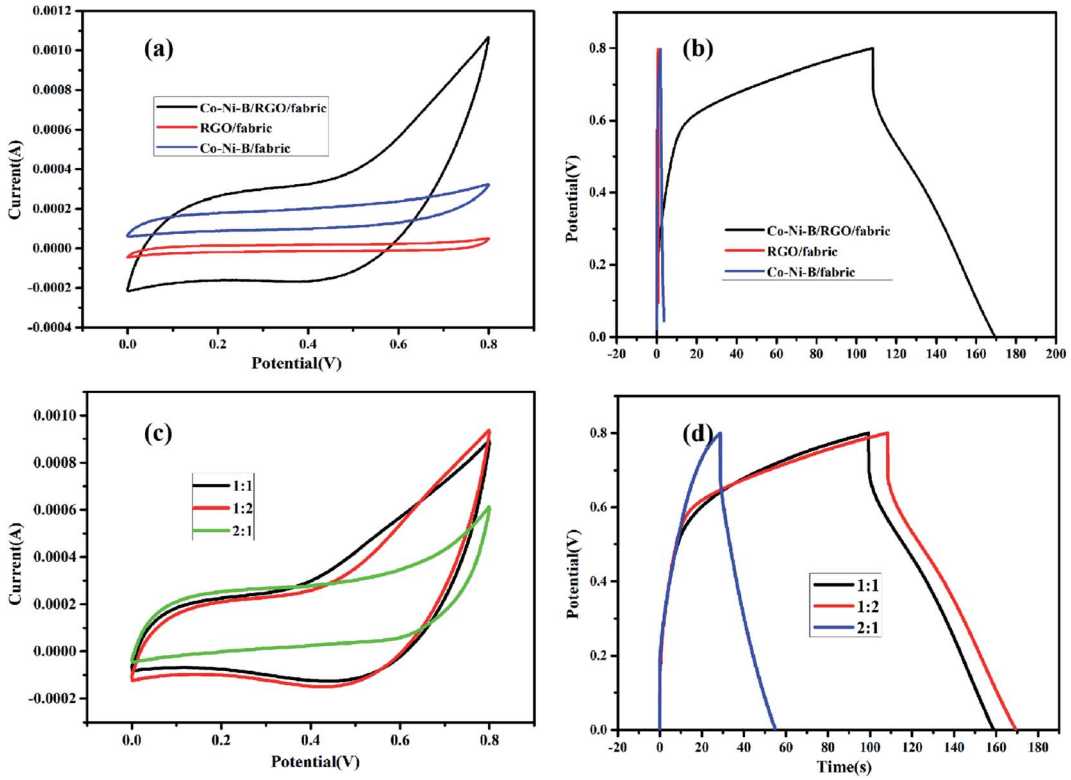

Fig. 7 (a) CV and (b) GCD curves of RGO/fabric, Co–Ni–B/RGO/fabric, and Co–Ni–B/fabric electrodes; (c) CV and (d) GCD curves of the as-made samples with different Co/Ni molar ratio.

previous reports, in addition to the merit of the disorder long-range atomic arrangement of Co–Ni–B amorphous materials leading to an outstanding electrochemical performance.[12,27]

Five elements, Ni, Co, B, C, and O, were detected in the XPS pattern, as shown in Fig. 6a, which was consistent with the EDS result. The binding energy peaks of Ni 2p (Fig. 6b) spectrum was measured at 855.7 eV, 862 eV, 873.5 eV, and 879.4 eV, attributable to Ni $2p_{3/2}$ and Ni $2p_{1/2}$, respectively,[11,28] thereby indicating elemental and oxidation states of nickel. The XPS peaks of Co 2p centered at 781.6 eV and 797 eV (Fig. 6c) were ascribed as Co $2p_{3/2}$ and Co $2p_{1/2}$, respectively. In addition, the other two peaks at 785 eV and 802.5 eV were assigned to shake-up satellite peaks.[11,12] This result verified that cobalt was in elemental and oxidation states. One typical peak at 191.5 eV, observed in the B 1s spectrum (Fig. 6d), corresponded to the oxidation state of boron, which confirmed the typical characteristics of amorphous metal borides exposed to air.[11,29] From Fig. 6e, four obvious peaks at 288.9 eV, 287.9 eV, 286.6 eV, and 284.5 eV detected in the C spectrum were ascribed to O–C=O, C=O, C–O, and C–C, respectively. In addition, one peak at 531.2 eV was found for absorbed O_2 in the O 1s spectra, as shown in Fig. 6f.

The effect of the electrode composition on electrochemical properties was studied with cyclic voltammogram and galvanostatic charge/discharge process. From CV curves and GCD tests (Fig. 7a and b), one can deduce that Co–Ni–B/RGO/fabric composite electrode exhibited the best electrochemical performance with the largest integral area and longest charge–discharge time due to the high conductivity of RGO and storage energy property of amorphous Co–Ni–B alloy.[11] The specific capacitance of RGO/cotton fabric resulted from the double-layer mechanism of RGO, whose weakness is the low capacity.[30,31] As for Co–Ni–B/fabric composite, its specific capacitance originated from the pseudocapacitance mechanism. However, the capacity was limited by the insulated cotton fabric substrate. In other words, the improved electrochemical property of Co-Ni-B/RGO/fabric was ascribed to the synergistic effect of conductive graphene sheets and high capacitance of amorphous Co–Ni–B alloy. Moreover, the special three-dimensional microstructure was beneficial for the ionic transfer for Co–Ni–B/RGO/fabric composite electrode.

The relationship between the molar ratio of Co/Ni and the electrochemical properties was also detected, and the result is shown in Fig. 7c and d. Clearly, the CV curve of Co1–Ni1–B/RGO/cotton fabric was nearly the same as that of Co1–Ni2–B/RGO/cotton fabric, while the closed circle area of Co2–Ni1–B/RGO/cotton fabric was the smallest. Also, the GCD curves of these three fabric electrodes were measured with a three-electrode system. Obviously, the charge–discharge time of Co2–Ni1–B/RGO/cotton fabric was shorter than those of Co1–Ni1–B/RGO/cotton fabric and Co1–Ni2–B/RGO/cotton fabric. It seems that the electrochemical performance of Co1–Ni2–B/RGO/cotton fabric was better than that of Co1–Ni1–B/RGO/cotton fabric due to the longer charge–discharge time. However, its coulombic efficiency was slightly behind the Co1–Ni1–B/RGO/cotton fabric.

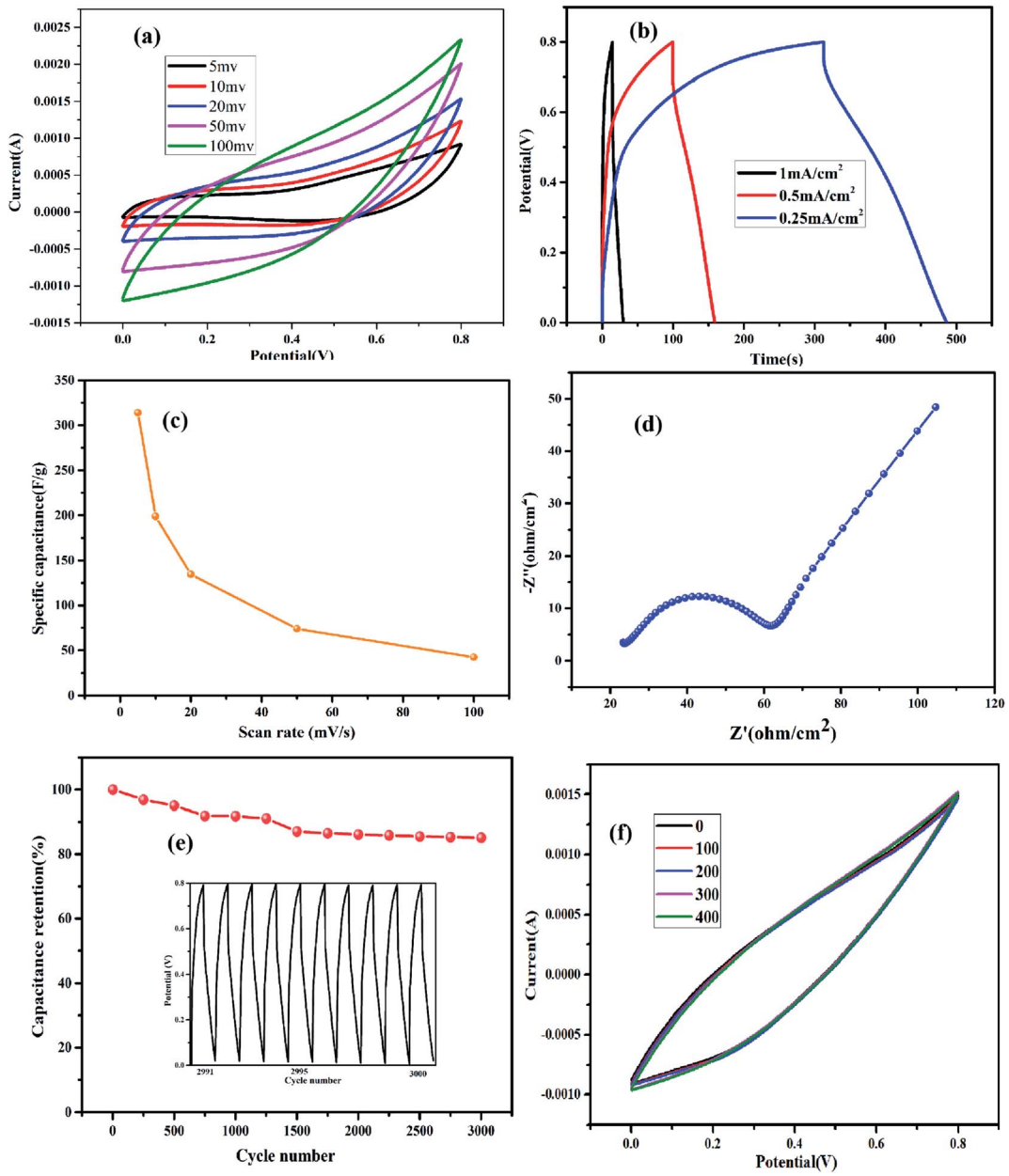

Fig. 8 (a) CV and (b) GCD curves of Co1–Ni1–B/RGO/fabric; (c) specific capacitance values calculated from CV curves with different scan rate; (d) electrochemical impedance spectroscopy; (e) cycle life test; (f) flexibility test.

Based on the analysis, Co1–Ni1–B/RGO/fabric exhibited a stable electrochemical property among these three fabric electrodes. Therefore, its electrochemical properties were systematically analysed. From Fig. 8a, no obvious pair of redox peaks was detected in all CV curves of Co1–Ni1–B/RGO/fabric electrode with different sweep rates ranging from 5 to 100 mV s^{-1}, thereby confirming its double-layer behaviour. All the GCD curves with different current densities in Fig. 8b were triangular in shape with the current density of 1 mA cm^{-2}, 0.5 mA cm^{-2}, and 0.25 mA cm^{-2}. The specific capacitance of Fig. 8c was calculated to be 313.9 F g^{-1}, 198.9 F g^{-1}, 134.4 F g^{-1}, 74 F g^{-1}, and 42.3 F g^{-1} at a scan rate of 5 mV s^{-1}, 10 mV s^{-1}, 20 mV s^{-1}, 50 mV s^{-1}, and 100 mV s^{-1}, respectively. Moreover, the specific capacitance from galvanic discharge curves was calculated as 276.9 F g^{-1}, 163.5 F g^{-1}, and 63.3 F g^{-1} when the discharge current was 0.25 mA cm^{-2}, 0.5 mA cm^{-2}, and 1 mA cm^{-2}, respectively. From Fig. 8d, the equivalent series resistance R_s value was 22.5 Ω, and charge transfer resistance R_{ct} value was 40 Ω, indicating the good electrical conductivity and fast reaction kinetics. Moreover, consecutive charging/discharging test at 1 mA cm^{-2} for 3000 cycles (Fig. 8e) revealed that this electrode retained 85.0% of initial specific capacitance, probably attributing to the synergistic effect of amorphous Co–Ni–B alloy and conducive RGO sheets. Also, this composite fabric electrode showed overlapped CV curves with variable bending–releasing cycles, as described in Fig. 8f. Even after 400 times, the CV curve of Co–Ni–B/RGO/fabric

electrode was nearly similar to that of the initial electrode, which indicated an ideal flexibility performance.

Conclusions

Co–Ni–B/RGO/fabric composite electrode was designed and fabricated *via* a facile and mild method at room temperature, normal pressure, and short reaction time, which helped in reducing the damage to cotton fabric caused by the harsh preparation conditions. Note that the three-dimensional architecture composed of Co–Ni–B nanosheets and RGO sheets guaranteed the fast diffusion of ions. With these special features, Co–Ni–B/RGO/fabric electrode showed a good electric capacity of 313.9 F g^{-1} with a scan rate of 5 mV s^{-1}. In addition, this fabric electrode showed proper stability with 85.0% retention of the specific capacitance after 3000 charge–discharge cycles.

Conflicts of interest

The authors declare that they have no known competing financial interests or personal relationships that could have appeared to influence the work reported in this paper.

Acknowledgements

The authors are grateful for the financial support of this research by "Natural Science Foundation of Jiangsu Province" (No. BK20181038) and "Jiangsu provincial government scholarship for studying abroad".

References

1 M. Tebyetekerwa, I. Marriam, Z. Xu, S. Y. Yang, H. Zhang, F. Zabihia, R. J. Jose, S. J. Peng, M. F. Zhu and S. Ramakrishna, *Energy Environ. Sci.*, 2019, **12**, 2148–2160.
2 Z. Q. Li, M. W. Tian, X. T. Sun, H. T. Zhao, S. F. Zhu and X. S. Zhang, *J. Alloys Compd.*, 2019, **782**, 986–994.
3 Z. X. Liu, F. N. Mo, H. F. Li, M. S. Zhu, Z. F. Wang, G. J. Liang and C. Y. Zhi, *Small Methods*, 2018, 1800124.
4 C. Sun, X. Li, Z. S. Cai and F. Y. Ge, *Electrochim. Acta*, 2019, **296**, 617–626.
5 L. B. Dong, C. J. Xu, Y. Li, C. L. Wu, B. Z. Jiang, Q. Yang, E. L. Zhou, F. Y. Kang and Q. H. Yang, *Adv. Mater.*, 2016, **28**, 1675–1681.
6 J. Heo, J. Eom, Y. H. Kim and S. K. Park, *Small*, 2018, **14**, 1703034.
7 Q. Qiu, M. M. Zhu, Z. L. Li, K. L. Qiu, X. Y. Liu, J. Y. Yu and B. Ding, *Nano Energy*, 2019, **58**, 750–758.
8 J. F. Sun, L. Z. Guo, X. Sun, J. Y. Zhang, L. R. Hou, L. Li, S. H. Yang and C. Z. Yuan, *Batteries Supercaps*, 2019, **2**, 820.
9 Y. Y. Shang, T. Xie, C. L. Ma, L. H. Su, Y. S. Gai, J. Liu and L. Y. Gong, *Electrochim. Acta*, 2018, **286**, 103–113.
10 X. X. Zhang, X. L. Zhang, G. M. Qu, Z. H. Wang, Y. R. Wei, J. M. Yin, G. T. Xiang and X. J. Xu, *Appl. Surf. Sci.*, 2020, **512**, 145621.
11 R. N. Chen, L. Liu, J. S. Zhou, L. Hou and F. M. Gao, *J. Power Sources*, 2017, **341**, 75–82.
12 Q. Z. Meng, W. Xu, S. L. Zhu, Y. Q. Liang, Z. D. Cui, X. J. Yang and A. Inoue, *Electrochim. Acta*, 2019, **296**, 198–205.
13 S. Wang, P. He, Z. W. Xie, L. P. Jia, M. Q. He, X. Q. Zhang, F. Q. Dong, H. H. Liu, Y. Zhang and C. X. Li, *Electrochim. Acta*, 2019, **296**, 644–652.
14 T. Q. Hao, J. Y. Sun, W. Wang and D. Yu, *Cellulose*, 2018, **25**, 4031–4041.
15 B. Wang, W. H. Song, P. Gu, L. H. Fan, Y. J. Yin and C. X. Wang, *Electrochim. Acta*, 2019, **297**, 794–804.
16 Y. Z. Li, Y. F. Zhang, H. R. Zhang, T. L. Xing and G. Q. Chen, *RSC Adv.*, 2019, **9**, 4180–4189.
17 M. A. P. Lima, J. J. Alcarazespinoza, F. A. G. D. Silva and H. P. D. Oliveira, *ACS Appl. Mater. Interfaces*, 2018, **10**, 13783–13795.
18 Y. K. Jeong, I. Son and S. H. Baek, *Appl. Surf. Sci.*, 2019, **467–468**, 963–967.
19 B. J. Liu, B. W. Zheng, Y. T. Wang, H. J. Li and W. Wang, *Cellulose*, 2020, **27**, 8813–8825.
20 W. Wang, T. Li, Y. Y. Sun, L. G. Liu, J. B. Wu, G. Yang and B. J. Liu, *Cellulose*, 2020, **27**, 7079–7092.
21 L. F. Shen, J. Wang, G. Y. Xu, H. S. Li, H. Dou and X. G. Zhang, *Adv. Energy Mater.*, 2015, **5**, 1400977.
22 L. L. Xu, M. X. Guo, S. Liu and S. W. Bian, *RSC Adv.*, 2015, **5**, 25244–25249.
23 A. Errokh, A. M. Ferraria, D. S. Conceicao, L. F. V. Ferreira, A. M. B. D. Rego, M. R. Vilar and S. Boufi, *Carbohydr. Polym.*, 2016, **141**, 229–237.
24 M. I. Sayyed, S. I. Qashou and Z. Y. Khattari, *J. Alloys Compd.*, 2017, **696**, 632–638.
25 H. H. Wei, K. Huang, L. Zhang, B. H. Ge, D. Wang, J. L. Lang, J. Y. Ma, D. Wang, S. Zhang, Q. Y. Li, R. Y. Zhang, N. Hussain, M. Lei, L. M. Liu and H. Wu, *Angew. Chem. Int. Ed.*, 2018, **57**, 3354–3359.
26 Y. Yang, L. Li, G. Ruan, H. Fei, C. Xiang, X. Fan and J. M. Tour, *ACS Nano*, 2014, **8**, 9622–9628.
27 Q. Li, Y. X. Xu, S. S. Zheng, X. T. Guo, H. G. Xue and H. Pang, *Small*, 2018, **14**, 1800426.
28 M. Q. Sheng, Q. Wu, Y. Wang, F. Liao, Q. Y. Zhou, J. X. Hou and W. P. Weng, *Electrochem. Commun.*, 2018, **93**, 104–108.
29 S. J. Qiu, J. L. Huang, F. H. Shen, R. Pang, H. L. Chu, Y. J. Zou, C. L. Xiang, F. Xu, Y. Du, J. C. Wang, L. X. Sun and H. Y. Zhou, *Int. J. Hydrogen Energy*, 2016, **41**, 3955–3960.
30 W. Wang, T. Li, K. Liu, S. Wang and H. X. Peng, *RSC Adv.*, 2020, **10**, 6249.
31 M. X. Guo, S. W. Bian, F. Shao, S. Liu and Y. H. Peng, *Electrochim. Acta*, 2016, **209**, 486–497.

